iScience

CellPress

Article

Enhanced Fermion Pairing and Superfluidity by an Imaginary Magnetic Field

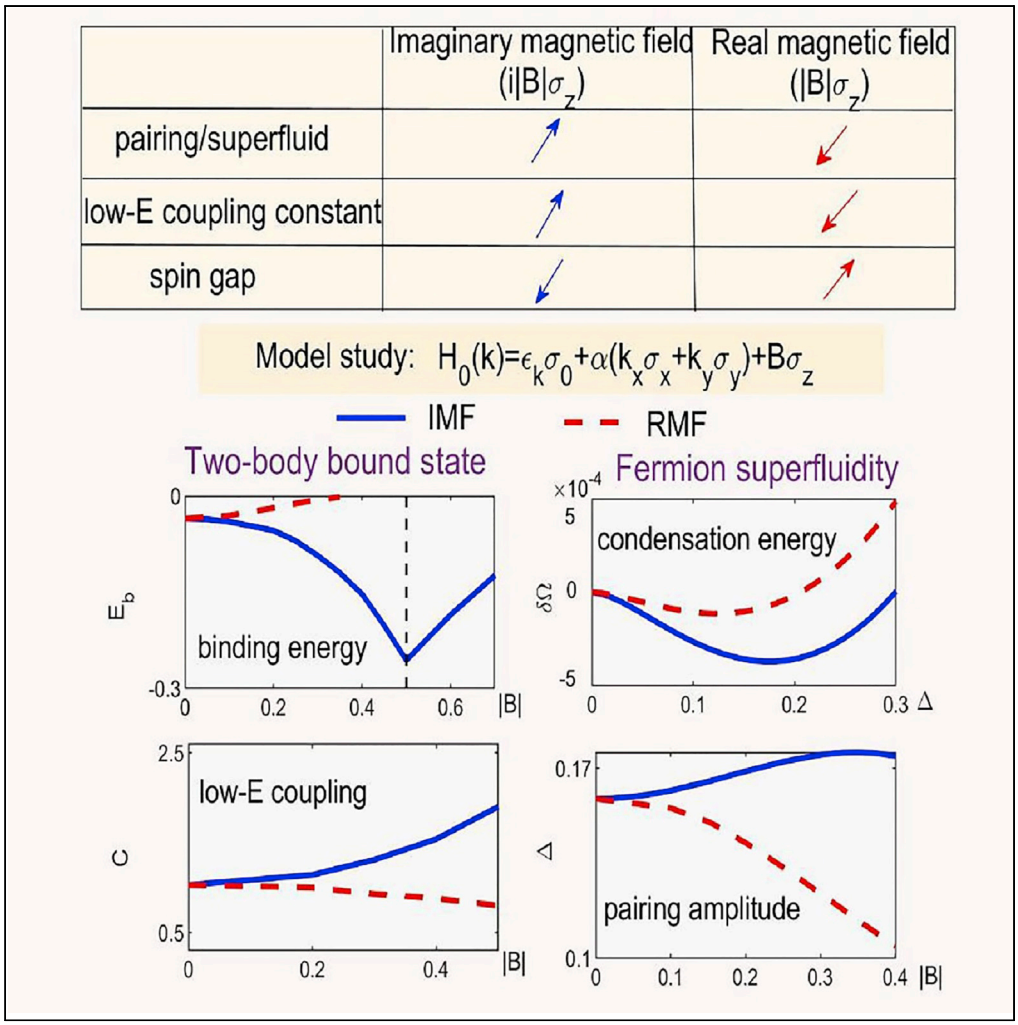

Lihong Zhou, Xiaoling Cui

xlcui@iphy.ac.cn

HIGHLIGHTS

We show an imaginary magnetic field can enhance the fermion pairing and superfluidity

We demonstrate above effect through exact two-body solutions and mean-field theory

We analyze the reason for such enhanced pairing superfluidity in fermion systems

Zhou & Cui, iScience *14*, 257–263
April 26, 2019 © 2019
https://doi.org/10.1016/j.isci.2019.03.031

iScience

CellPress

Article

Enhanced Fermion Pairing and Superfluidity by an Imaginary Magnetic Field

Lihong Zhou[1] and Xiaoling Cui[1,2,3,*]

SUMMARY

We show that an imaginary magnetic field (IMF), which can be generated in non-Hermitian systems with spin-dependent dissipations, can greatly enhance the s-wave pairing and superfluidity of spin-1/2 fermions, in distinct contrast to the effect of a real magnetic field. The enhancement can be attributed to the increased coupling constant in low-energy space and the reduced spin gap in forming singlet pairs. We have demonstrated this effect in a number of different fermion systems with and without spin-orbit coupling, using both the two-body exact solution and many-body mean-field theory. Our results suggest an alternative route toward strong fermion superfluid with high superfluid transition temperature.

INTRODUCTION

Searching for strong fermion superfluids and their underlying mechanisms has been one of the central tasks in condensed matter and cold atomic physics. In cold atoms, a prominent example for strong superfluid is the unitary Fermi gas, where the s-wave scattering length diverges and the interaction energy solely scales with the Fermi energy (DeMarco and Jin, 1999; Giorgini et al., 2008; Zwierlein, 2014). Apart from resonant interaction, several other factors have also been shown to induce strong pairing and superfluidity, such as low dimension (Feld et al., 2011; Sommer et al., 2012; Murthy et al., 2018), large effective range (Hazlett et al., 2012; Ho et al., 2012; Qi and Zhai, 2012), highly symmetric spin-orbit coupling (Vyasanakere and Shenoy, 2011; Vyasanakere et al., 2011; Gong et al., 2011; Hu et al., 2011; Yu and Zhai, 2011; Cui, 2012; Zhang et al., 2012a, 2012b; Wu and Yu, 2013; Wang and Greene, 2015; Guan and Blume, 2016), etc. On the contrary, the presence of a magnetic field or spin imbalance is generally believed to reduce and even destroy the pairing superfluidity, especially when the spin gap overcomes the pairing strength.

In this work, we report another efficient tool for generating strong pairing superfluid, namely, an imaginary magnetic field (IMF). Experimentally, the IMF can be realized in non-Hermitian atomic systems by laser-assisted spin-selective dissipations (Li et al., 2019; Lapp et al., 2018). Consider the spin-1/2($\uparrow,\downarrow$) system; the IMF can be equivalently achieved by applying a laser field uniquely to spin-$\downarrow$ atom, which is resonantly coupled to a highly excited atomic state and causes loss. This spin-dependent loss can be described by a potential $i\Gamma\sigma_z$ up to a constant energy shift ($\sim -i\Gamma/2$), where Γ determines the loss rate. Such potential exactly plays the role of an imaginary Zeeman energy due to an imaginary magnetic field $B = i\Gamma$. Here we show that the IMF can greatly enhance the s-wave pairing and superfluidity of spin-1/2 fermions, behaving just oppositely to a real magnetic field (RMF). Consider a Rashba spin-orbit-coupled (SOC) fermion system as an example; we find that even a small IMF can induce an exponential enhancement of the two-body binding energy in weak coupling regime and the enhancement equally holds for the pairing superfluid of many fermions in all interaction regimes. We further demonstrate that the IMF-enhanced pairing commonly exists in several other typical fermion systems, with different types of SOC and even without SOC. The enhancement can be attributed to the increased coupling constant in low-energy space and the reduced spin gap in forming singlet pairs when an IMF is present. These results, which are detectable in current cold atoms experiment, suggest an alternative route toward strong fermion superfluid with high superfluid transition temperature.

RESULTS AND DISCUSSION

To demonstrate the effect of an IMF, we start with a concrete model of spin-1/2 fermions($\uparrow,\downarrow$) with Rashba SOC. The single-particle Hamiltonian in momentum ($\mathbf{k}$) space can be written as ($\hbar = 1$ throughout the article)

$$h_0(\mathbf{k}) = \epsilon_{\mathbf{k}}\sigma_0 + \alpha\left(k_x\sigma_x + k_y\sigma_y\right) + B\sigma_z, \qquad \text{(Equation 1)}$$

[1]Beijing National Laboratory for Condensed Matter Physics, Institute of Physics, Chinese Academy of Sciences, Beijing 100190, China

[2]Songshan Lake Materials Laboratory, Dongguan, Guangdong 523808, China

[3]Lead Contact

*Correspondence: xlcui@iphy.ac.cn

https://doi.org/10.1016/j.isci.2019.03.031

This is an open access article under the CC BY-NC-ND license (http://creativecommons.org/licenses/by-nc-nd/4.0/).

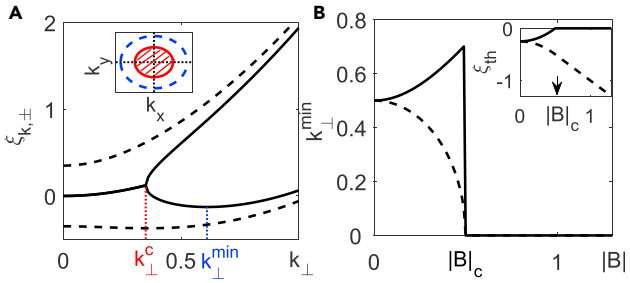

Figure 1. Single Particle Physics under Rashba SOC and IMF/RMF

(A) Real parts of single-particle spectra under a Rashba SOC and an IMF (solid lines) or an RMF (dashed lines). Here we take $k_z = 0$, and IMF/RMF with the same strength $|B| = 0.35E_0$. Inset: exceptional ring (red solid circle, with radius $k_\perp^c$) and the location of energy minimum (blue dashed circle, with radius $k_\perp^{min}$) in (k_x,k_y) plane in the case of IMF.

(B) Location of energy minimum, $k_\perp^{min}$, as a function of $|B|$ for IMF (solid line) and RMF (dashed line). Inset shows the corresponding threshold energy (in the real part) ξ_{th}. For IMF, $k_\perp^{min}$ shows a discontinuity and accordingly ξ_{th} shows a kink at $|B|_c = 0.5E_0$. In all plots, the units of momentum and energy are, respectively, k_0 and E_0. (Color online.)

here $\epsilon_{\mathbf{k}} = \mathbf{k}^2/(2m)$; σ_0 and $\sigma_{x,y,z}$ are, respectively, the identity and Pauli matrices; α is the strength of Rashba SOC, which naturally defines a momentum scale $k_0 = 2m\alpha$ and an energy scale $E_0 = 2m\alpha^2$; and B can be real or imaginary, respectively, denoting an RMF or an IMF. The eigen energies of (1) are

$$\xi_{\mathbf{k},\pm} = \epsilon_{\mathbf{k}} \pm \sqrt{\alpha^2 k_\perp^2 + B^2}, \qquad \text{(Equation 2)}$$

where $\pm$ is the helicity index and $k_\perp = \sqrt{k_x^2 + k_y^2}$. Note that in writing Equation 1 with an imaginary B, we have utilized the effective non-Hermitian Hamiltonian reduced from the Lindblad equation, by neglecting a term that induces quantum jumps between diagonal density matrixes in different particle-number sectors. It has been argued that such process will not affect the physical quantities produced with a given particle number (Nakagawa et al., 2018; Zhou and Yu, 2019).

Equation 2 results in distinct single-particle spectra for IMF and RMF, as displayed in Figure 1A. For RMF, all $\xi_{\mathbf{k},\pm}$ are real, and a gap is opened at $\mathbf{k} = 0$, whereas for an IMF, $\xi_{\mathbf{k},\pm}$ are complex (conjugate to each other) for $k_\perp < k_\perp^c \equiv |B|/\alpha$ and purely real for $k_\perp > k_\perp^c$. Right at $k_\perp = k_\perp^c$, both the two levels and two eigenstates coalesce, forming an exceptional ring in (k_x,k_y) plane; see the red solid circle in the inset of Figure 1A. Note that as the size of this ring does not depend on k_z, in 3D $\mathbf{k}$-space it forms an exceptional surface as of a straight cylinder along z. In Figure 1B, we plot the location of energy minimum, denoted by $k_\perp^{min}$, as varying $|B|$. For RMF, $k_\perp^{min}$ continuously decreases to zero as increasing B. For IMF, $k_\perp^{min}$ first increases with $|B|$ following $\sim (k_0/2)\sqrt{1+4|B|^2/E_0^2}$, as shown by the larger blue dashed circle in the inset of Figure 1A, whereas at a critical $|B|_c = 0.5E_0$, it jumps to zero, signifying a first-order transition. Accordingly, at the transition point the energy threshold (ξ_{th}) moves from finite $k_\perp^{min}$ to $\mathbf{k} = 0$ and exhibits a kink, as shown in the inset of Figure 1B.

Now we come to the two-body problem, where two fermions interact under contact potential $U = g\delta(\mathbf{r})P_{S=0}$; here $\mathbf{r}$ is the relative motion, $P_{S=0}$ is the projection operator of spin singlet state $|S=0\rangle = \frac{|\uparrow\downarrow\rangle - |\downarrow\uparrow\rangle}{\sqrt{2}}$, and the bare coupling g can be related to the s-wave scattering length a_s via $1/g = m/(4\pi a_s) - 1/V\sum_{\mathbf{k}} 1/2\epsilon_{\mathbf{k}}$. The two-body results are shown in Figure 2.

In Figure 2A, we plot the two-body binding energy E_b as a function of $1/a_s$ for IMF and RMF with the same amplitude $|B|$. When compared with the zero B case, the application of an IMF will enhance $|E_b|$ at all couplings, whereas RMF always reduce $|E_b|$. The picture is more clearly shown in Figure 2B, where E_b is plotted as a function of $|B|$ at given $1/a_s$. We can see that on increasing $|B|$ from zero, in RMF case the bound state quickly vanishes with $E_b \to 0$, whereas the IMF can support deeper bound state (with decreasing E_b) until $|B|$ reaches $|B|_c$, when the single-particle threshold ξ_{th} displays a kink (see Figure 1B). To highlight the dramatic effect of IMF in favoring bound states, in Figure 2C we plot the minimum E_b (at $|B| = |B|_c$) as functions of $1/a_s$, when compared with that without IMF. We can see that the IMF effect is visible in all interaction regimes from weak to strong couplings. For instance, for a weak coupling $1/(a_s k_0) = -1$, at $|B|_c$ we have $|E_b|/E_0 = 0.115$, about 20 times larger than the value (0.005) at $B = 0$.

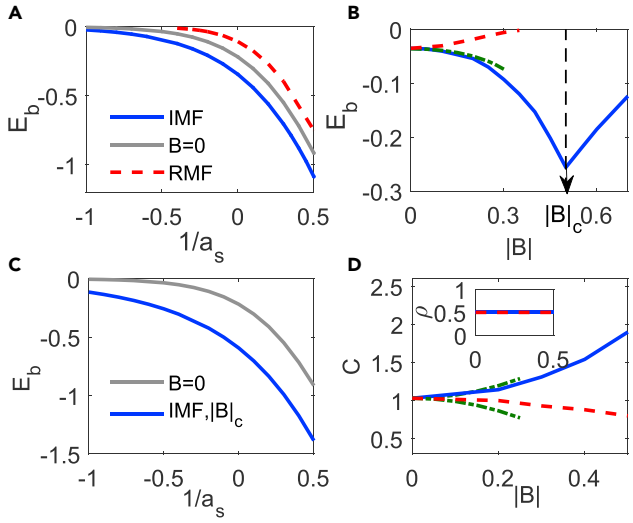

Figure 2. Two-body Bound State under Rashba SOC and IMF/RMF

(A) Two-body binding energy E_b with Rashba SOC as a function of $1/a_s$ for IMF (blue solid line) and RMF (red dashed line) with $|B|/E_0 = 0.3$, when compared with $B = 0$ (gray line).

(B) E_b as a function of $|B|$ for IMF (blue solid) and RMF (red dashed line) given a fixed $1/(a_s k_0) = -0.5$. Green dash-dotted line shows fit to Equation 4 for IMF (B^2<0). Under IMF, E_b reaches minimum at $|B|_c$.

(C) Minimum E_b under IMF (blue solid line) as function of $1/a_s$, when compared with the zero B case (gray line).

(D) Coupling constants C between two threshold fermions as functions of $|B|$ for IMF (blue solid line) and RMF (red dashed line), and the inset shows threshold DoS ρ. Green dash-dotted lines show analytical fit (see text). (Color online.)

Physically, the enhanced bound state is associated with the IMF-increased coupling strength between low-energy states. To demonstrate this, we rewrite the two-body equation (see Methods) as

$$\frac{1}{g} = \int d\varepsilon \rho(\varepsilon) \frac{C(\varepsilon)}{E - \varepsilon}, \qquad \text{(Equation 3)}$$

where $\rho(\epsilon)$ and $C(\epsilon)$, respectively, denote the density of state (DoS) and the coupling constant for two particles at scattering energy ϵ. The change of these two values as varying B directly determines the fate of bound state. It can be more transparently seen through in weak coupling limit, where the bound state formation is dominated by the low-energy scattering near $E \sim 2\xi_{th}$. In Figure 2D and its inset, we plot C and ρ at threshold $E = 2\xi_{th}$ as varying $|B|$. We can see that whereas ρ keeps static constant, C can increase (decrease) with $|B|$ in the case of IMF (RMF). Indeed, at small B, C can be expanded as $C(B) = C(0)(1 - 4B^2/E_0^2)$, consistent with the numerical result shown in Figure 2D. Then based on Equation (3), we arrive at the following expansion of E_b in weak coupling limit ($(k_0 a_s)^{-1} \to -\infty$) and with small B ($|B| \ll E_0$):

$$E_b(B) = E_b(0) \exp\left(-\frac{16B^2}{E_0^2} \frac{1}{k_0 |a_s|} \right), \qquad \text{(Equation 4)}$$

here $E_b(0)$ is the binding energy at $B = 0$. Most remarkably, Equation 4 shows that by applying an IMF ($B^2 < 0$), $|E_b|$ can *exponentially* increase with a *huge* coefficient due to $1/(k_0|a_s|) \gg 1$. In contrast, applying an RMF ($B^2 > 0$) will exponentially reduce $|E_b|$. We have confirmed that Equation 4 matches well with numerical results at small $|B|$, as shown by the dash-dotted line in Figure 2B.

Inspired by the two-body result, we now turn to the property of pairing superfluid for many fermions. Under the mean-field Bardeen-Cooper-Schrieffer (BCS) theory, we introduce the paring order parameter $\Delta = (g/V)\sum_{\mathbf{k}} L\langle c_{-\mathbf{k}\downarrow} c_{\mathbf{k}\uparrow}\rangle R$ and $\tilde{\Delta} = (g/V)\sum_{\mathbf{k}} L\langle c^{\dagger}_{\mathbf{k}\uparrow} c^{\dagger}_{-\mathbf{k}\downarrow}\rangle R$, where $c_{\mathbf{k}\sigma}$ is the annihilation operator of a free fermion of spin-σ at $\mathbf{k}$, and $|\rangle_{R(L)}$ refers to the right (left) eigenvector for the BCS ground state. By some algebra, the thermodynamic potential $\Omega = H - \mu N$ can be diagonalized as

$$\Omega = \sum_{\mathbf{k}}{}' \left(\sum_{i=1}^{4} E_{ki} \alpha^{R\dagger}_{ki} \alpha^{L}_{ki} + 2(\epsilon_{\mathbf{k}} - \mu) \right) - \frac{\Delta\tilde{\Delta}}{g}. \qquad \text{(Equation 5)}$$

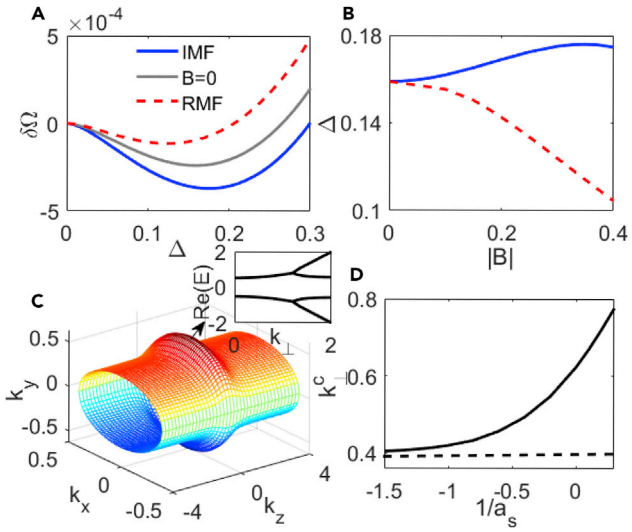

Figure 3. Fermion Superfluid under Rashba SOC and IMF/RMF at a Given $\mu = -0.05E_0$

(A) Thermodynamic potential Ω as a function of Δ for IMF (blue solid line) and RMF (red dashed line) with $|B| = 0.3E_0$, when compared with that with $B = 0$ (gray line).

(B) Pairing amplitude Δ as varying $|B|$ for IMF (blue solid line) and RMF (red dashed line). In both (A,B), we take $1/(k_0 a_s) = -0.5$.

(C) $\mathbf{k}$-space exceptional surface for quasi-particles at resonance and with IMF strength $|B| = 0.4E_0$. Inset shows the real parts of quasi-particle energies evolving with $k_\perp$ at fixed $k_z = 0$, which split at $k_\perp^c$.

(D) $k_\perp^c$ as a function of $1/a_s$ at given $|B| = 0.4E_0$. Horizontal dashed line shows $k_\perp^c$ for free particles. (Color online.)

Here $\alpha_{\mathbf{k}i}^{R\dagger}$ ($\alpha_{\mathbf{k}i}^{L}$) is the creation (annihilation) operator of the i-th right (left) quasi-particle with momentum $\mathbf{k}$, which satisfies the anti-commutation relation $\{\alpha_{\mathbf{k}i}^{R\dagger}, \alpha_{\mathbf{k}'j}^{L}\} = \delta_{\mathbf{k}\mathbf{k}'}\delta_{ij}$; the four quasi-particle energies follow

$$E_{\mathbf{k}} = \pm\sqrt{A_{\mathbf{k}} + B_{\mathbf{k}} \pm 2\sqrt{A_{\mathbf{k}}B_{\mathbf{k}} - (\alpha k_\perp)^2\Delta\tilde{\Delta}}}, \qquad \text{(Equation 6)}$$

with $A_{\mathbf{k}} = (\epsilon_{\mathbf{k}} - \mu)^2 + \Delta\tilde{\Delta}$, $B_{\mathbf{k}} = \alpha^2 k_\perp^2 + B^2$. In contrast to the case of RMF where all $E_{\mathbf{k}i}$ are real, in the presence of an IMF they can be real or complex, depending on the values of $\mathbf{k}$ and other parameters Δ, $\tilde{\Delta}$, μ, etc. As only the product $\Delta\tilde{\Delta}$ matters in the functional Ω, but not individual Δ or $\tilde{\Delta}$, in the following we will choose a special case with $\Delta = \tilde{\Delta}$ and minimize Ω (which is real) in terms of Δ to find the ground state.

In Figure 3A, we show the typical landscapes of $\Omega(\Delta)$ for both IMF and RMF with a given strength $|B|$. It can be seen that compared with the zero B case, the IMF (RMF) can shift the minimum of Ω to larger (smaller) Δ, and accordingly $\Omega_{\min}$ is further decreased (increased), indicating a stronger (weaker) fermion superfluid. In Figure 3B, we further plot the ground state Δ, which indeed is an increasing function of $|B|$ for IMF, contrarily to the case of RMF. We have checked that these conclusions will not be qualitatively altered by the change of a_s and μ.

In the above discussion, we have shown the dramatic effect of non-Hermitian potential (the IMF) to interacting fermions. In turn, the interaction effect can also alter the non-Hermitian property, in that the exceptional surface (ES) can be largely deformed from the free particle case. In Figure 3C, we show the $\mathbf{k}$-space ES of quasi-particles, which is determined by

$$A_{\mathbf{k}}B_{\mathbf{k}} = (\alpha k_\perp)^2\Delta\tilde{\Delta}. \qquad \text{(Equation 7)}$$

This equation predicts that two pairs of quasi-particles (see Equation 6) coalesce simultaneously at ES, with two separate energies $E_{\mathbf{k}} = \pm\sqrt{A_{\mathbf{k}} + B_{\mathbf{k}}}$, as shown in the inset of Figure 3C. When compared with the free particle case where ES is a straight cylinder along z (see Figure 1), here the ES can be deformed, as shown by Figure 3C, and the deformation is pronounced at low-energy space where the pairing takes a dominant role. Upon increasing the interaction strength, more and more momentum states will be strongly affected by pairing and ES will get even more distorted and extend to larger $k_\perp$, as manifested by the increasing $k_\perp^c$ for quasi-particles shown in Figure 3D.

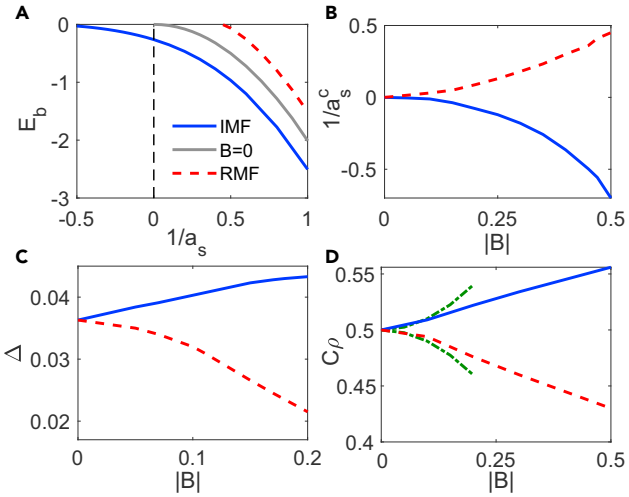

Figure 4. Pairing and Superfluidity under 1D SOC with IMF/RMF

(A) Two-body binding energy E_b as functions of $1/a_s$ for IMF (blue solid line) and RMF (red dashed line) with $|B| = 0.5E_0$, when compared with that with $B = 0$ (gray line).

(B) Critical $1/a_s$ to support a two-body bound state as varying $|B|$ for IMF (blue solid line) and RMF (red dashed line).

(C) Many-body pairing amplitude Δ as a function of $|B|$ for IMF (blue solid line) and RMF (red dashed line). Here we take $1/(k_0 a_s) = -0.5$ and $\mu = -0.05E_0$.

(D) Product of coupling constant C and DoS ρ for two threshold fermions as varying $|B|$. Green dash-dotted lines show analytical fit (see text). (Color online.)

To this end, we have demonstrated the enhanced pairing and superfluidity by an IMF for fermions with Rashba SOC. Next we show that such effect equally applies to other fermion systems, and in particular, we choose two types of single-particle Hamiltonians as below:

$$\text{(I)} \quad h_0(\mathbf{k}) = \epsilon_{\mathbf{k}}\sigma_0 + \alpha k_x \sigma_x + B\sigma_z;$$
$$\text{(II)} \quad h_0(\mathbf{k}) = \epsilon_{\mathbf{k}}\sigma_0 + \beta\sigma_x + B\sigma_z$$

When compared with the highly symmetric Rashba SOC as described by Equation 1, here we consider in case (I) a 1D SOC that has much less symmetry and in case (II) a simple transverse field without any SOC. Given their distinct structures, these three cases belong to the most typical situations for the non-trivial effect of IMF or RMF. In practice, case (I) with a real B has been realized using the two-photon Raman process (Lin et al., 2011; Zhang et al., 2012a, 2012b; Wang et al., 2012; Cheuk et al., 2012; Qu et al., 2013), and the transverse field in (II) and IMF in both (I,II) can be implemented, respectively, by the radio-frequency (RF) field and laser-assisted dissipation.

For case (I), we have carried out the two-body and many-body calculations for the pairing and superfluidity therein, which also show enhancement by IMF; see Figure 4. In particular, with an IMF, the two-body bound state can form even in the weak coupling regime with $1/a_s<0$, in contrary to the case of RMF where it can only appear in the molecule side with $1/a_s>0$ (Williams et al., 2013; Zhang et al., 2013; Kurkcuoglu and de Melo, 2016); see Figure 4A. In Figure 4B, we plot the critical $1/a_s^c$ for the bound-state formation as a function of $|B|$, and we see that the larger the IMF is, the weaker is the coupling (i.e., smaller $1/a_s^c$) required to afford a bound state, whereas the RMF displays an opposite trend. Consistent with these two-body results, the many-body calculation shows the IMF-enhanced pairing amplitude Δ, in contrast to the case of RMF; see Figure 4C. The enhancement again can be understood from the analyses of low-energy coupling strength C and DoS ρ. In this case, we have $C(B)$ behaving the same as in Rashba SOC case, whereas $\rho(B)$ varies as $\sim\rho(0)\ (1+2B^2/E_0^2)$, therefore $\rho(B)C(B) = \rho(0)C(0)\ (1-2B^2/E_0^2)$, which increases (decreases) with $|B|$ for an IMF (an RMF) as shown in Figure 4D. Compared with the Rashba SOC case, here the magnitude of enhancement in 1D SOC is smaller due to the IMF-reduced DoS.

For case (II), the situation is much simpler, as the spin (σ) and orbit ($\mathbf{k}$) are fully decoupled in the single-particle level. Now there is only one factor left, i.e., the spin gap, to influence the pairing and superfluidity properties.

From the spin spectrum $\epsilon_{\pm} = \pm\sqrt{\beta^2 + B^2}$, we define the spin gap as $G = \sqrt{\beta^2 + B^2}$. Obviously, increasing $|B|$ in IMF and RMF cases will have different effects to G, i.e., in the former G increases, whereas in the latter G decreases, until becoming zero at $|B| = \beta$, where the exceptional point is located. Such behavior can directly influence the many-body superfluidity. Indeed, the mean-field BCS theory gives quasi-particle spectra as:

$$E_k = \pm\sqrt{(\epsilon_k - \mu)^2 + \Delta^2} \pm G, \qquad \text{(Equation 8)}$$

which shows that the spin gap G directly plays the role of an effective magnetic field h_{eff} in pairing problem. As it is known that changing h_{eff} can result in a sequence of quantum phase transitions between normal and various pairing phases across resonances (Sheehy and Radzihovsky, 2006; Pao et al., 2006; Hu and Liu, 2006; Parish et al., 2007), such transitions can be equally induced by changing the IMF strength $|B|$. For trapped fermions, this effect directly leads to a tunable phase separation between normal and BCS pairing states, which can be measured directly as previously in spin-imbalanced Fermi gas (Zwierlein et al., 2006; Partridge et al., 2006).

In conclusion, we have demonstrated the enhanced pairing and superfluidity by an IMF in a number of distinct fermion systems with and without SOC, by which we expect the same IMF effect can extend to a wide class of fermion systems. We have revealed the underlying mechanism for such enhancement as the IMF-increased low-energy coupling strength and IMF-reduced spin gap in forming singlet pairs. The remarkably opposite effects generated by an IMF and an RMF could be detected in cold atom experiments. In particular, the binding energy of molecules can be measured by RF spectroscopy, and the pairing superfluidity can be probed by momentum-resolved RF spectroscopy (Stewart et al., 2007; Gaebler et al., 2010). Finally, although in this work we have only concentrated on the ground-state property at zero temperature, our results immediately suggest an equally strong superfluid at finite temperature and with a high superfluid transition temperature (T_c). This may also offer an alternative perspective toward the high-T_c superconductor ever studied in literature.

METHODS

All methods can be found in the accompanying Transparent Methods supplemental file.

SUPPLEMENTAL INFORMATION

Supplemental Information can be found online at https://doi.org/10.1016/j.isci.2019.03.031.

ACKNOWLEDGMENTS

We thank Wei Yi for helpful discussions. This work is supported by the National Key Research and Development Program of China (2018YFA0307600, 2016YFA0300603) and the National Natural Science Foundation of China (Nos.11622436, 11421092, and 11534014).

AUTHOR CONTRIBUTIONS

X.C. conceived the project and supervised the study. L.Z. performed the numerical calculations and analyzed the data. All authors contributed to writing the manuscript.

DECLARATION OF INTERESTS

The authors declare no competing interests.

Received: January 6, 2019
Revised: February 27, 2019
Accepted: March 28, 2019
Published: April 26, 2019

REFERENCES

Cheuk, L.W., Sommer, A.T., Hadzibabic, Z., Yefsah, T., Bakr, W.S., and Zwierlein, M.W. (2012). Spin-injection spectroscopy of a spin-orbit coupled fermi gas. Phys. Rev. Lett. *109*, 095302.

Cui, X. (2012). Mixed partial-wave scattering with spin-orbit coupling and validity of pseudo-potentials. Phys. Rev. A *85*, 022705.

DeMarco, B., and Jin, D.S. (1999). Onset of fermi degeneracy in a trapped atomic gas. Science *285*, 1703.

Feld, M., Fröhlich, B., Vogt, E., Koschorreck, M., and Köhl, M. (2011). .Observation of a pairing pseudogap in a two-dimensional Fermi gas. Nature *480*, 75.

Gaebler, J.P., Stewart, J.T., Drake, T.E., Jin, D.S., Perali, A., Pieri, P., and Strinati, G.C. (2010). Observation of pseudogap behavior in a strongly interacting Fermi gas. Nat. Phys. *6*, 569.

Giorgini, S., Pitaevskii, L.P., and Stringari, S. (2008). Theory of ultracold atomic Fermi gases. Rev. Mod. Phys. *80*, 1215.

Gong, M., Tewari, S., and Zhang, C. (2011). BCS-BEC crossover and topological phase transition in 3D spin-orbit coupled degenerate fermi gases. Phys. Rev. Lett. *107*, 195303.

Guan, Q., and Blume, D. (2016). Scattering framework for two particles with isotropic spin-orbit coupling applicable to all energies. Phys. Rev. A *94*, 022706.

Hazlett, E.L., Zhang, Y., Stites, R.W., and O'Hara, K.M. (2012). Realization of a resonant fermi gas with a large effective range. Phys. Rev. Lett. *108*, 045304.

Ho, T.-L., Cui, X., and Li, W. (2012). Alternative route to strong interaction: narrow feshbach resonance. Phys. Rev. Lett. *108*, 250401.

Hu, H., Jiang, L., Liu, X.J., and Pu, H. (2011). Probing anisotropic superfluidity of rashbons in atomic Fermi gases. Phys. Rev. Lett. *107*, 195304.

Hu, H., and Liu, X.J. (2006). Mean-field phase diagrams of imbalanced Fermi gases near a Feshbach resonance. Phys. Rev. A *73*, 051603(R).

Kurkcuoglu, D.M., and de Melo, C.A.R.S. (2016). Formation of Feshbach molecules in the presence of artificial spin-orbit coupling and Zeeman fields. Phys. Rev. A *93*, 023611.

Lapp, S., Ang'ong'a, J., Alex An, F., and Gadway, B. (2018). Engineering tunable local loss in a synthetic lattice of momentum states. arxiv, 1811.06046.

Li, J., Harter, A.K., Liu, J., de Melo, L., Joglekar, Y.N., and Luo, L. (2019). Observation of parity-time symmetry breaking transitions in a dissipative Floquet system of ultracold atoms. Nat. Commun. *855*, 1.

Lin, Y.-J., Jiménez-García, K., and Spielman, I.B. (2011). SpinCorbit-coupled BoseCEinstein condensates. Nature *471*, 83.

Murthy, P.A., Neidig, M., Klemt, R., Bayha, Boettcher, L.I., Enss, T., Holten, M., Zürn, G., Preiss, P.M., and Jochim, S. (2018). High temperature pairing in a strongly interacting two-dimensional Fermi gas. Science *359*, 452.

Nakagawa, M., Kawakami, N., and Ueda, M. (2018). Non-Hermitian Kondo effect in ultracold alkaline-earth atoms. Phys. Rev. Lett. *121*, 203001.

Pao, C.H., Wu, S.T., and Yip, S.K. (2006). Superfluid stability in BEC-BCS crossover. Phys. Rev. B *73*, 132506.

Parish, M.M., Marchetti, F.M., Lamacraft, A., and Simons, B.D. (2007). Finite temperature phase diagram of a polarised Fermi condensate. Nat. Phys. *3*, 124.

Partridge, G.B., Li, W., Kamar, R.I., Liao, Y., and Hulet, R.G. (2006). Pairing and phase separation in a polarized fermi gas. Science *311*, 503.

Qi, R., and Zhai, H. (2012). Highly polarized fermi gases across a narrow feshbach resonance. Phys. Rev. A. *85*, 041603(R).

Qu, C., Hamner, C., Gong, M., Zhang, C., and Engels, P. (2013). Observation of Zitterbewegung in a spin-orbit-coupled bose-einstein condensate. Phys. Rev. A *88*, 021604(R).

Sheehy, D.E., and Radzihovsky, L. (2006). BEC-BCS crossover in "magnetized" Feshbach-resonantly paired superfluids. Phys. Rev. Lett. *96*, 060401.

Sommer, A.T., Cheuk, L.W., Ku, M.J.H., Bakr, W.S., and Zwierlein, M.W. (2012). Evolution of fermion pairing from three to two dimensions. Phys. Rev. Lett. *108*, 045302.

Stewart, J.T., Gaebler, J.P., and Jin, D.S. (2007). Using photoemission spectroscopy to probe a strongly interactiong Fermi gas. Nature *454*, 744.

Vyasanakere, J.P., and Shenoy, V.B. (2011). How does a synthetic non-Abelian gauge field influence the bound states of two spin-half fermions? Phys. Rev. B *83*, 094515.

Vyasanakere, J.P., Zhang, S., and Shenoy, V.B. (2011). BCS-BEC crossover induced by a synthetic non-Abelian gauge field. Phys. Rev. B *84*, 014512.

Wang, S.-J., and Greene, C.H. (2015). General ultracold scattering formalism with isotropic spin orbit coupling. Phys. Rev. A *91*, 022706.

Wang, P., Yu, Z.-Q., Fu, Z., Miao, J., Huang, L., Chai, S., Zhai, H., and Zhang, J. (2012). Spin-orbit coupled degenerate fermi gases. Phys. Rev. Lett. *109*, 095301.

Williams, R.A., Beeler, M.C., LeBlanc, L.J., Jimenez-Garcia, K., and Spielman, I.B. (2013). A Raman-induced Feshbach resonance in an effectively single-component Fermi gas. Phys. Rev. Lett. *111*, 095301.

Wu, Y., and Yu, Z. (2013). Short range asymptotic behavior of the wave-functions of interacting spin-half fermionic atoms with spin-orbit coupling: a model study. Phys. Rev. A *87*, 032703.

Yu, Z.Q., and Zhai, H. (2011). Spin-orbit coupled fermi gases across a feshbach resonance. Phys. Rev. Lett. *107*, 195305.

Zhang, P., Zhang, L., and Zhang, W. (2012a). Interatomic collisions in two-dimensional and quasi-two-dimensional confinements with spin-orbit coupling. Phys. Rev. A *86*, 042707.

Zhang, J.-Y., Ji, S.-C., Chen, Z., Zhang, L., Du, Z.-D., Yan, B., Pan, G.-S., Zhao, B., Deng, Y.-J., Zhai, H., et al. (2012b). Collective dipole oscillations of a spin-orbit coupled bose-einstein condensate. Phys. Rev. Lett. *109*, 115301.

Zhang, L., Deng, Y., and Zhang, P. (2013). Scattering effective interactions of ultracold atoms with spin-orbit coupling. Phys. Rev. A *87*, 053626.

Zhou, Z., and Yu, Z. (2019). Interaction effects on PT-symmetry breaking transition in atomic gases. arxiv, 1901.01174.

Zwierlein, M.W. (2014). Novel Superfluids (Oxford University Press), pp. 269–422.

Zwierlein, M.W., Schirotzek, A., Schunck, C.H., and Ketterle, W. (2006). Fermionic superfluidity with imbalanced spin populations and the quantum phase transition to the normal state. Science *311*, 492.

ISCI, Volume *14*

Supplemental Information

Enhanced Fermion Pairing and Superfluidity by an Imaginary Magnetic Field

Lihong Zhou and Xiaoling Cui

Supplemental Information

Enhanced fermion pairing and superfluidity by an imaginary magnetic field

Lihong Zhou and Xiaoling Cui

Transparent Methods

In this section we provide more details about how to exactly solve the two-body bound state and many-body superfluid.

Two-body bound state: The two-body problem can be solved by using the Lippman-Schwinger equation $|\Psi\rangle = G_E U|\Psi\rangle$, where Ψ is the two-body wave function. We then arrive at the following equation for binding energy $E_b = E - 2\xi_{th}$:

$$\frac{1}{g} = \langle S=0|G_E(0,0)|S=0\rangle,$$

where the Green function reads

$$G_E(\mathbf{r},\mathbf{r}') = \frac{1}{2}\sum_{\mathbf{k};\mu\nu=\pm} \frac{\langle \mathbf{r}|\mathbf{k}^R_\mu;-\mathbf{k}^R_\nu\rangle\langle -\mathbf{k}^L_\nu;\mathbf{k}^L_\mu|\mathbf{r}'\rangle}{\langle \mathbf{k}^L_\mu|\mathbf{k}^R_\mu\rangle\langle -\mathbf{k}^L_\nu|-\mathbf{k}^R_\nu\rangle(E-\xi_{\mathbf{k}\mu}-\xi_{-\mathbf{k}\nu})}.$$

Here $|\mathbf{k}^R_\mu\rangle$ and $|\mathbf{k}^L_\mu\rangle$ refer to the left and right eigenvectors defined through $h_0|\mathbf{k}^R_\mu\rangle = \xi_{\mathbf{k}\mu}|\mathbf{k}^R_\mu\rangle$ and $h_0^\dagger|\mathbf{k}^L_\mu\rangle = \xi^*_{\mathbf{k}\mu}|\mathbf{k}^L_\mu\rangle$. In principle, for the case of IMF the expansion in G_E fails at the exceptional ring where there is only one eigenstate for each $\mathbf{k}$. Nevertheless, the integrand in G_E behaves smoothly across the exceptional region, and thus its presence has no effect to the two-body solution. For the case of RMF, we have $h_0 = h_0^\dagger$, $\xi_{\mathbf{k}\mu} = \xi^*_{\mathbf{k}\mu}$ and $|\mathbf{k}^R_\mu\rangle = |\mathbf{k}^L_\mu\rangle$.

Many-body system: For the many-body pairing, under the mean-field theory we can write the thermodynamic potential Ω as

$$\Omega = \sum_{\mathbf{k}}{}' \Big(F^\dagger_{\mathbf{k}}\Omega(\mathbf{k})F_{\mathbf{k}} + 2(\epsilon_{\mathbf{k}}-\mu)\Big) - \frac{\Delta\tilde{\Delta}}{g},$$

with $F_{\mathbf{k}} = (c_{\mathbf{k}\uparrow}, c^\dagger_{-\mathbf{k}\downarrow}, c^\dagger_{-\mathbf{k}\uparrow}, c_{\mathbf{k}\downarrow})^T$, and $\Omega(\mathbf{k})$ is

$$\begin{pmatrix} \epsilon_{\mathbf{k}}-\mu+B & \Delta & 0 & \alpha k_\perp e^{-\imath\phi_k} \\ \tilde{\Delta} & -\epsilon_{\mathbf{k}}+\mu+B & \alpha k_\perp e^{-\imath\phi_k} & 0 \\ 0 & \alpha k_\perp e^{\imath\phi_k} & -\epsilon_{\mathbf{k}}+\mu-B & -\tilde{\Delta} \\ \alpha k_\perp e^{\imath\phi_k} & 0 & -\Delta & \epsilon_{\mathbf{k}}-\mu-B \end{pmatrix}.$$

Note that the summation over $\mathbf{k}$ in Ω is carried out only over half of $\mathbf{k}$-space. By diagonalizing the 4×4 matrix at each $\mathbf{k}$, we can obtain the form of Ω as Eq.(5) in the main text, and the associated quasi-particle energy as Eq.(6) in the main text.

At zero temperature, we have $\Omega = \sum_{\mathbf{k}}{}' \Big(\sum_{i=1}^4 E_{\mathbf{k}i}\Theta\big(-Re(E_{\mathbf{k}i})\big) + 2(\epsilon_{\mathbf{k}}-\mu)\Big) - \Delta\tilde{\Delta}^2/g$, where $\Theta(x) = 1$ if $x>0$ and $=0$ otherwise. The ground state of the system can be found by minimizing Ω as a function of the product $\Delta\tilde{\Delta}$, given $a_s,\ \mu,\ B$ all fixed. In the main text we have chosen a special case with $\Delta = \tilde{\Delta}$.